

# Response of Jupiter's auroras to conditions in the interplanetary medium as measured by the Hubble Space Telescope and Juno

J. D. Nichols<sup>1</sup>, S. V. Badman<sup>2</sup>, F. Bagenal<sup>3</sup>, S. J. Bolton<sup>4</sup>, B. Bonfond<sup>5</sup>, E. J. Bunce<sup>1</sup>, J. T. Clarke<sup>6</sup>, J. E. P. Connerney<sup>7</sup>, S. W. H. Cowley<sup>1</sup>, R. W. Ebert<sup>4</sup>, M. Fujimoto<sup>8</sup>, J.-C. Gérard<sup>5</sup>, G. R. Gladstone<sup>4</sup>, D. Grodent<sup>5</sup>, T. Kimura<sup>9</sup>, W. S. Kurth<sup>10</sup>, B. H. Mauk<sup>11</sup>, G. Murakami<sup>12</sup>, D. J. McComas<sup>13</sup>, G. S. Orton<sup>14</sup>, A. Radioti<sup>5</sup>, T. S. Stallard<sup>1</sup>, C. Tao<sup>15</sup>, P. W. Valek<sup>4</sup>, R. J. Wilson<sup>3</sup>, A. Yamazaki<sup>12</sup>, I. Yoshikawa<sup>16</sup>

<sup>1</sup>Department of Physics and Astronomy, University of Leicester, University Road, Leicester, LE1 7RH, UK

<sup>2</sup>Department of Physics, Lancaster University, LA1 4YB, UK

<sup>3</sup>Laboratory for Atmospheric and Space Physics, University of Colorado Boulder, Boulder, Colorado, USA

<sup>4</sup>Southwest Research Institute, San Antonio, Texas, USA

<sup>5</sup>Laboratory for Planetary and Atmospheric Physics, Université de Liège, Institut d'Astrophysique et de Géophysique - B5c,

Allée du 6 aout, 17, B-4000 Liège, Belgium

<sup>6</sup>725 Commonwealth Avenue, Center for Space Physics, Boston University, Boston, MA 02215, USA

<sup>7</sup>Goddard Space Flight Center, Greenbelt, Maryland, USA

<sup>8</sup>Institute of Space and Astronautical Science, Japan Aerospace Exploration Agency, Sagami, Japan

<sup>9</sup>Nishina Center for Accelerator-Based Science, RIKEN, RIBF403, 2-1, Hirosawa, Saitama, Japan

<sup>10</sup>Department of Physics and Astronomy, University of Iowa, Iowa City, IA 52241, USA

<sup>11</sup>Johns Hopkins University Applied Physics Laboratory, 11100 Johns Hopkins Road, Laurel, MD 20723, USA

<sup>12</sup>Institute of Space and Astronautical Science, Japan Aerospace Exploration Agency, Sagami, Japan

<sup>13</sup>Princeton Plasma Physics Laboratory, P.O. Box 451, Princeton, NJ 08543-0451, USA

<sup>14</sup>Jet Propulsion Laboratory, M/S 169-237, 4800 Oak Grove Drive, Pasadena, CA 91109, USA

<sup>15</sup>Space Environment Laboratory, National Institute of Information and Communications Technology, Tokyo, Japan

<sup>16</sup>Department of Complexity Science and Engineering, University of Tokyo, Kashiwa, Japan

## Key Points:

- We present the first comparison of Jupiter's auroras with an extended and complete set of near-Jupiter interplanetary data.
- During compressions, the well-defined sector of Jupiter's emission and the dusk poleward region brightened, the latter pulsating.
- The power emitted from the noon active region did not exhibit dependence on any interplanetary parameter, though the morphology changed.

**Abstract**

We present the first comparison of Jupiter’s auroral morphology with an extended, continuous and complete set of near-Jupiter interplanetary data, revealing the response of Jupiter’s auroras to the interplanetary conditions. We show that for  $\sim 1$ -3 days following compression region onset the planet’s main emission brightened. A duskside poleward region also brightened during compressions, as well as during shallow rarefaction conditions at the start of the program. The power emitted from the noon active region did not exhibit dependence on any interplanetary parameter, though the morphology typically differed between rarefactions and compressions. The auroras equatorward of the main emission brightened over  $\sim 10$  days following an interval of increased volcanic activity on Io. These results show that the dependence of Jupiter’s magnetosphere and auroras on the interplanetary conditions are more diverse than previously thought.

**1 Introduction**

The dynamics of Jupiter’s magnetosphere are dominated by planetary rotation and the outflow of material from Io [see e.g. *Khurana et al.*, 2004; *Clarke et al.*, 2004], and the nature of the solar wind interaction has long been debated [*Brice and Ioannidis*, 1970; *Southwood and Kivelson*, 2001; *Nichols et al.*, 2006; *Badman and Cowley*, 2007; *McComas and Bagenal*, 2007; *Cowley et al.*, 2008; *Delamere and Bagenal*, 2010]. Observationally, the total power of the jovian auroras in various wavelengths exhibits modulation by interplanetary conditions [*Baron et al.*, 1996; *Pryor et al.*, 2005; *Clarke et al.*, 2009; *Badman et al.*, 2016; *Kita et al.*, 2016; *Kimura et al.*, 2016; *Dunn et al.*, 2016], particularly increasing in some cases (not all) in response to expected solar wind compression regions characterised by overall high dynamic pressure and interplanetary magnetic field (IMF) strength.

The detailed morphological response of the far-ultraviolet auroras to the interplanetary medium has been examined previously using the Hubble Space Telescope (HST) and near-Jupiter spacecraft by *Nichols et al.* [2007, 2009a], the former study comparing HST images with Cassini flyby observations, and the latter with New Horizons solar wind data and interplanetary measurements extrapolated from Earth orbit using a magnetohydrodynamic model. These studies showed that in response to expected compression region onset the main emission sometimes brightened in the narrow region with System III longitude  $\lambda_{III} > 180^\circ$  (usually observed in the dawn sector by HST), whereas, in contrast the emission at smaller longitudes was neither bright nor well-defined. However, intense arcs poleward of the main emission were observed during estimated compression regions for around 2 days following estimated compression region onset. An important limitation of those studies, however, was that they were hampered by relying on either limited HST or interplanetary observations, or interplanetary data extrapolated from Earth that carried significant timing uncertainties. Further, those HST observations were obtained using either fixed  $\sim 100$  s exposure times, or time-tag exposures of less than 5 minutes, both of which limit characterisation of fast-varying auroral forms. In 2016 the NASA Juno spacecraft approached and entered into orbit around Jupiter (with orbit insertion on 5 July 2016), providing a full and continuous complement of near-Jupiter solar wind and IMF data. During this interval we observed Jupiter’s FUV auroras using the HST Space Telescope Imaging Spectrograph (STIS) for 47 orbits from 16 May to 18 July, primarily using  $\sim 45$  min time-tag imaging exposures. In this paper we examine this unique combination of data in order to determine the response of Jupiter’s auroras to conditions in the interplanetary medium. We show that Jupiter’s auroral response to interplanetary conditions is more diverse than previously understood.

## 2 Data

### 2.1 Hubble Space Telescope observations

We obtained 44 orbits of FUV time-tag imaging and 3 orbits of FUV time-tag spectroscopy using the HST/STIS Multi-Anode Microchannel Array detector over the interval May to July 2016. When imaging, we used the F25SRF2 filter, which admits H<sub>2</sub> Lyman and Werner bands. Observations were obtained with a cadence of roughly one orbit per 24 h (with some exceptions that contained 2 or 3 orbits) in 3 groups: DoYs 137-159, 174-182, and 193-200. We concentrate here only on images of the northern auroras obtained during Juno approach, DoY 137-182, yielding 32 orbits. Raw images were extracted from the time-tag data using integration and increment times of 30 s and 10 s, respectively, and images were then processed using the extensively-used Boston University pipeline that has been discussed in detail previously [e.g. *Clarke et al.*, 2009; *Nichols et al.*, 2009a]. Here, intensity was converted from counts to kR of total un-absorbed H<sub>2</sub> emission in the 70-180 nm bandwidth using the conversion factors of *Gustin et al.* [2012] (assuming a fiducial color ratio of 2.5; resultant powers are larger than reported by *Clarke et al.* [2009] owing to the larger waveband considered). All images obtained in this program are shown in the supporting information (SI). Total emitted power and powers from different regions were extracted and corrected for viewing geometry using the method detailed by *Nichols et al.* [2009a], and times account for one-way light travel time.

### 2.2 Juno interplanetary data

We employ Juno interplanetary data presented and discussed in detail by *McComas et al.* [2017]; *Wilson and al* [2017]. Specifically, we use 60 s resolution data in RTN coordinates from the fluxgate magnetometer (FGM) [*Connerney et al.*] and plasma moments computed by *Wilson and al* [2017] using data from the Jovian Auroral Distributions Experiment (JADE) instrument [*McComas et al.*, 2013]. We compute the magnitude of the IMF in the plane perpendicular to the radial vector, i.e.  $B_{\perp} = \sqrt{B_T^2 + B_N^2}$ , and the clock-angle  $\theta_c$  of the IMF relative to the jovian magnetic axis (thus with 0° indicating northward field, positive toward dawn), using the method detailed by *Nichols et al.* [2006]. We employ solar wind velocity  $v_{sw}$  and dynamic pressure  $p_{sw}$  measurements, using the latter to compute the magnetopause and bow shock stand-off distances,  $R_{mp}$  and  $R_{bs}$ , respectively, using the model of *Joy et al.* [2002]. The low-latitude dayside reconnection voltage  $\phi_{LL}$  is then computed using the algorithm of *Nichols et al.* [2006], i.e.  $\phi_{LL} = v_{sw} B_{\perp} L_0 \cos^4(\theta_c/2)$ , where  $L_0$  is the width of the channel in the solar wind that reconnects, taken to be  $R_{mp}/2$ .

We estimate the time of impact on the ionosphere using the method of *Nichols et al.* [2007], which considers 3 timescales. Briefly, these are (a) solar wind transport time given by the distance along the Sun-planet line between the position of the observed IMF phase front, calculated from Juno's position by using the mean Parker spiral angle of 11°, and  $R_{bs}$  as calculated above (b) the magnetosheath traversal time computed assuming a linear decrease in velocity from that just downstream of the shock, i.e.  $0.26v_{sw}$  to that just upstream of the magnetopause, assumed to be  $30 \text{ km s}^{-1}$ , and (c) the time for disturbances to travel along outer magnetosphere field lines to the ionosphere via Alfvén waves. The overall lag/lead time varies between  $\sim -5 \text{ h}$  (i.e. leading) and  $\sim 3 \text{ h}$ .

## 3 Results

The data discussed in Section 2 are plotted in Figure 1, while selected representative HST images are shown in Figure 2. We first note from Figure 1a that the viewing geometry-corrected UV powers observed by HST are typically in the range  $\sim 1\text{-}3 \text{ TW}$ , with the notable exception of an event at  $\sim 02 \text{ h}$  on DoY 142, during which HST observed a maximum UV power of  $\sim 5.5 \text{ TW}$ , the most powerful auroras observed by the telescope to date. For comparison, we also plot values obtained contemporaneously by the EXCEED

instrument on the JAXA Hisaki satellite, provided by *Kimura and et al.* [2017]. The Hisaki powers are also corrected for viewing geometry and scaled to the same bandwidth of the HST values (see *Tao et al.* [2016] for further information). Hisaki UV powers broadly concur with HST observations, though with increased temporal coverage which indicated that the power continued to rise still further on DoY 142 to  $\sim 8.5$  TW before dropping to  $\sim 2.1$  TW at the time of the second HST observation on DoY 142 at  $\sim 2130$  h. Other notable enhancements of the total power up to values of  $\sim 2$  TW occurred on DoYs 146, 151, 154, 175, 176, and 182, while a short-lived enhancement between HST orbits was observed by Hisaki on DoY 158.

The interplanetary data shown in Figures 1b-g indicates that the field was  $B_T$ -dominated as expected at  $\sim 5$  AU and that three solar wind compression regions were incident on Jupiter's magnetosphere during these intervals, separated by rarefaction regions of varying depth. The first compression was an interplanetary coronal mass ejection while the others were corotating interaction regions associated with crossings of the heliospheric current sheet. The observed times of the forward (reverse) shocks of these compressions are given by *McComas et al.* [2017], while the propagated times are  $\sim 1000$  h on DoY 141 ( $\sim 0000$  h on DoY 147),  $\sim 1500$  h on DoY 149 ( $\sim 0000$  h on DoY 155), and  $\sim 0100$  h on DoY 173. Details about the interplanetary data can be found in *McComas et al.* [2017] and *Wilson and al* [2017] but briefly, the compressions (colored blue in Figure 1) were characterised by high IMF strengths ( $\sim 1$ -3 nT) and dynamic pressures ( $\sim 2$ - $5 \times 10^{-1}$  nPa), and accordingly low estimated magnetopause standoff distance  $\sim 70$   $R_J$ . The rarefactions observed were either shallow (colored cyan, with IMF strengths  $\sim 0.5$ - $0.7$  nT and dynamic pressures of order  $\sim 10^{-2}$  nPa) or deep (colored yellow, with IMF strengths  $\sim 0.1$ - $0.2$  nT and dynamic pressures down to  $\sim 2 \times 10^{-3}$  nPa). The estimated magnetopause standoff distance varied in response, with values between up to  $\sim 130$   $R_J$ . The solar wind velocity overall varied between  $\sim 370$   $\text{km s}^{-1}$  to  $\sim 530$   $\text{km s}^{-1}$  with large increases associated with the forward shocks of the compressions. Finally, the estimated low latitude dayside reconnection voltage was generally larger during the compression regions and where the IMF turned northward, with values of  $\sim 1$ -3 MV in the compression regions,  $\sim 0.4$  MV in the shallow initial rarefaction, and  $\sim 0.2$  MV in the deep rarefaction. It is also worth noting that an enhancement in Jupiter's sodium nebula was observed on DoY 140, coincidentally near the time of the observed first forward shock in this interval, [M. Yoneda, personal communication, 2017], and possibly associated with an eruption observed on Io on DoY 138 [K. de Kleer, personal communication, 2017].

It is first evident that all three forward shocks observed are accompanied by an enhancement of the total emitted UV power over  $\sim 1$ -3 days following the onset of the compression regions, and the extreme event on DoY 142 also follows a few hours after the sodium nebula enhancement. The power did not remain uniformly high during compressions, however, dropping to  $\sim 1$  TW after a few days, and increasing toward the end of the first two compressions. On the basis of its morphology, discussed below, the brightening on DoY 182 was also likely associated with the onset of a compression region. We have calculated the Pearson correlation coefficients for the UV powers and interplanetary parameters smoothed with a boxcar width of one planetary rotation. A full table of results is shown in the SI, but here we restrict discussion to coefficients  $r_{xy}$  with significance  $p < 0.05$ , yielding in this case the correlation with  $B_{\perp}$  ( $r, p$ ) $_{P_{UV} B_{\perp}} = (0.45, 0.023)$  as the only significant value.

Considering now the auroral morphology, representative images are shown in Figure 2, corresponding to the times labeled at the top of Figure 1. The powers from regions delimited by the yellow lines in Figure 2 are shown in Figure 3. These comprise two active regions observed poleward of the main emission, the well-defined portion of the main emission over  $\lambda_{III} > 170^{\circ}$ , and the equatorward region over  $\lambda_{III} < 190^{\circ}$ . Though the regions are fixed in  $\lambda_{III}$ , the well-defined main emission (WDME) region is typically observed by HST near dawn, the equatorward region near dusk, while the two poleward regions are in the dusk and noon sectors, hence termed here 'dusk active region' (DAR) and 'noon active region' (NAR) respectively. We consider only the well-defined region of the

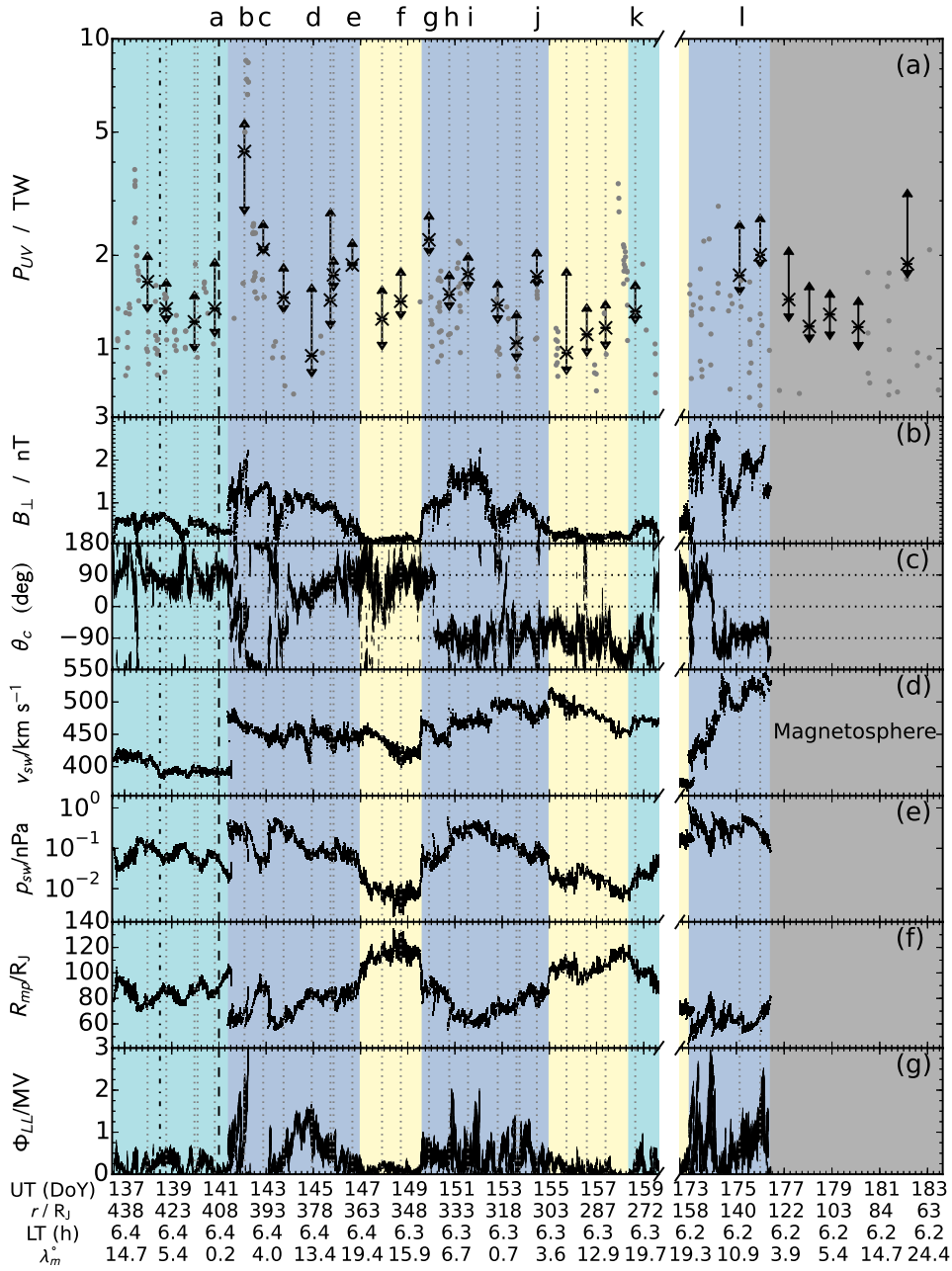


**Figure 1.** Plot showing auroral powers and interplanetary data versus UT at the ionosphere. We show (a) median and range of total UV powers  $P_{UV}$  in TW observed by HST in each orbit (black crosses with error bars) along with powers observed by Hisaki (gray points); (b)  $B_{\perp}$  in nT; (c) IMF clock angle  $\theta_c$  in degrees along with horizontal dotted lines at 0 and  $\pm 90^\circ$ ; (d)  $v_{sw}$  in  $\text{km s}^{-1}$ ; (e)  $\rho_{sw}$  in nPa; (f)  $R_{mp}$  in  $R_J$ ; and finally (g)  $\Phi_{LL}$  in MV. Vertical dotted lines indicate the times of the HST observations. Also shown by the vertical dashed and dot-dashed lines are times of an observed eruption on Io and sodium nebula enhancement, respectively. The colors indicate different interplanetary conditions as discussed in the text, and the gray box indicates where Juno left the solar wind. The letters at the top correspond to the times of the images shown in Figure 2.

main emission since the often unstructured nature of the auroras at smaller longitudes introduces ambiguity as to what is part of the main emission. We neglect low latitude emission at  $\lambda_{III} > 190^\circ$  to avoid contamination by bright, expanded dawn storm emissions. It is worth noting first that increased overall power in compressions arises from both intense few- to a few tens of MR emission along the WDME and pulsed forms in the dusk and occasionally noon active regions. The DAR specifically exhibited bright, strongly-pulsed emission during all three compressions and the initial shallow rarefaction conditions. The emission in this region typically (but not always) took the form of pulsing patches or arcs parallel to the main oval. A striking feature of such an arc observed on DoY 142 (Figure 2c) is that it marked the boundary between bright  $\sim$ few-hundred kR emission on the dusk side and an unusually large dark polar region that was not evident in images obtained less than 20 h previously. The pulsed nature of the DAR emission is shown in Figure 4 for 8 representative compression observations. These pulsations were either irregular and bursty (e.g. as in Figs. 4a and h), or quasi-periodic, similar to those discussed recently by *Bonfond et al.* [2017], though we note that here we discuss power emitted in a fixed region, rather than identifying individual pulsating forms. As with those authors, however, we observe periods of  $\sim$ 3 min (e.g. Figs. 4c and d) but also longer periods, such as  $\sim$ 6 min (Figure 4f) or  $\sim$ 11 min (Figure 4b and g). Interestingly, in the second compression, the peaks in the spectral power tended to broaden and move toward longer periods over DoYs 151-154 (Figs. 4d-g) as also evident in the overall powers in Figure 3a. In general, the DAR power broadly decreased during the compressions from large  $\sim$ 100 GW values to  $\sim$ 50 GW, and the DAR was typically less active during rarefactions. An exception to this occurred during the initial shallow rarefaction, when the DAR exhibited bright and variable emission, though more disordered and with fewer pulsed arc or patch structures. Overall, significant correlations are with  $B_\perp$  ( $(r, p)_{P_{UV\,DAR}\,B_\perp} = (0.59, 0.002)$ ) and magnetopause size ( $(r, p)_{P_{UV\,DAR}\,R_{mp}} = (-0.51, 0.010)$ ).

Turning now to the NAR, the powers for which are shown in Figure 3b, highly variable emission was observed during both rarefactions (e.g. Figure 2a and f) and compressions (e.g. Figure 2l), such that no significant correlations are observed with any interplanetary parameters. However, the morphology was somewhat different between the two cases, as exemplified by images f and l. In the rarefactions, the emission in the NAR comprised multiple, transient spots of emission extending throughout the NAR and often up into higher latitudes. Occasionally, the emission formed a poleward arc at noon, similar to the ‘inner ovals’ discussed previously [*Pallier and Prangé, 2001; Grodent et al., 2003; Nichols et al., 2009b; Stallard et al., 2016*]. In the compressions, the variable emission in the NAR typically comprised noonward extents of pulsating DAR emission though resembling more the rarefaction region morphology toward the end of the first compression.

Considering now the WDME, the emitted powers for which are shown in Figure 3c, the power did not stay uniformly high throughout the compression regions, decaying in the first compression from the  $\sim$ 1.8 TW dawn storm observed by HST (Figure. 2b) to  $\sim$ 100 GW in  $\sim$ 1 day, and varying in the second between  $\sim$ 320, 100 and 400 GW in images g, h, and i, before dropping back to  $\sim$ 160 GW. Toward the ends of both the first and second compressions, the region of the WDME exhibited high powers, though in these cases the emission was dominated by bright, patchy emission extending to lower latitudes in the case of image e (discussed further below), and a second dawn storm in the case of image j. The two observations during the third compression (e.g. image l) exhibited elevated powers of  $\sim$ 450 GW, but there was limited temporal coverage during this event. The power emitted from the WDME during the final observation on DoY 182 was high at  $\sim$ 600 GW, and this combined with the powerful, bursty  $\sim$ 200 GW DAR emission implies these images were obtained during another compression. During the rarefactions, the WDME was typically dim as shown in e.g. Figure 2f and k. It is also interesting to note that there were unusually low intensities (a few 10s of kR) on the dusk side of the main oval in image f. Finally, it is worth mentioning that the statistical main oval for this program (see the SI for a table of coordinates) is  $\sim$ 2° equatorward of the 2007 statistical oval in the ‘kink’ region.

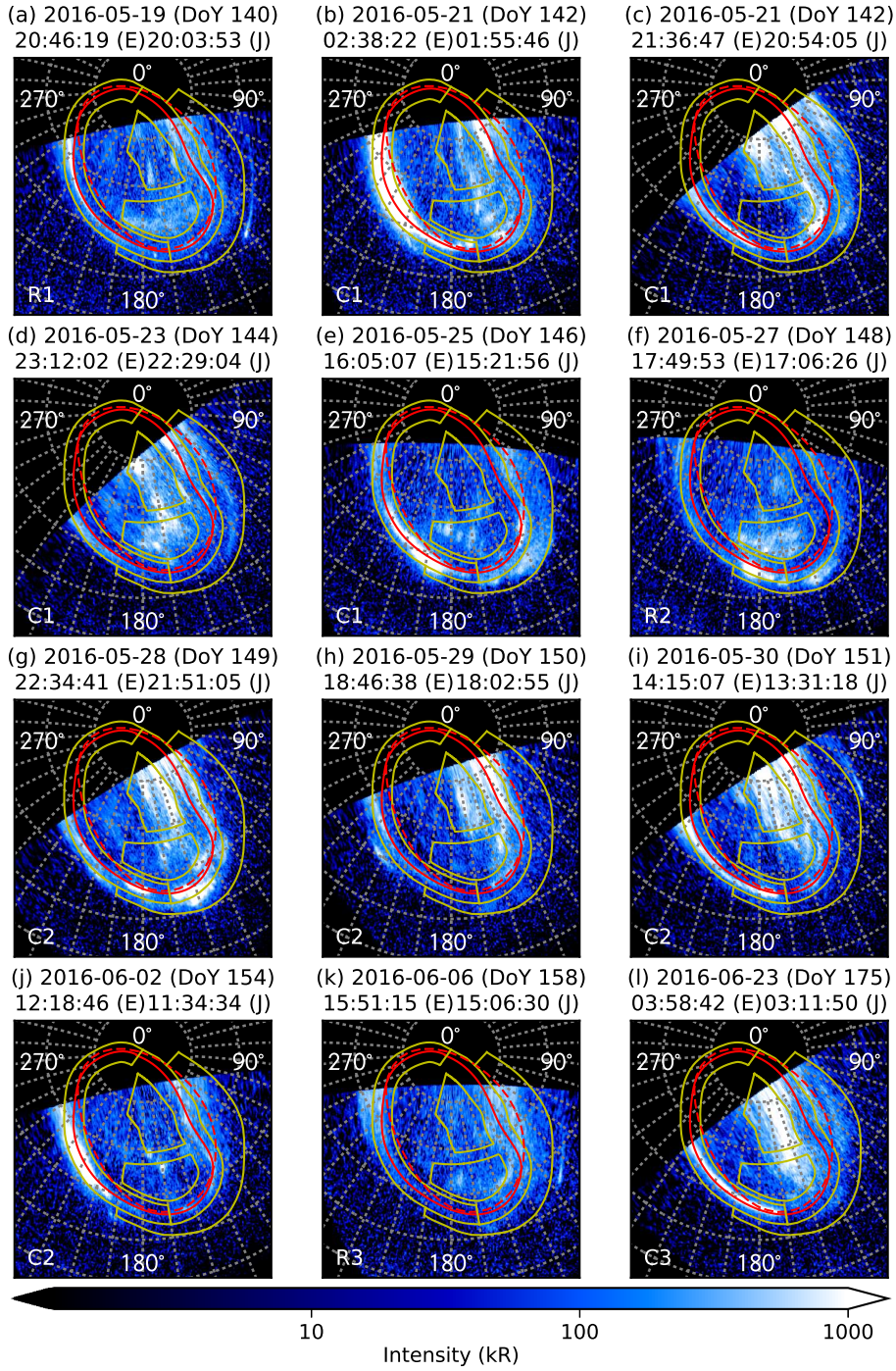


**Figure 2.** Representative projected images, shown with a  $10^\circ \times 10^\circ$  graticule and  $\lambda_{III} = 180^\circ$  directed toward the bottom. Red lines show the statistical oval for this program (solid) and the 30 R<sub>J</sub> VIP4 oval [Connerney *et al.*, 1981, 1998] (dashed). The yellow lines denote the areas from which powers were extracted. Each image is labelled with the time of observation (E) and the time of emission (J). Labels in the bottom left refer to the interplanetary conditions, R1 denoting the first rarefaction, C2 the second compression etc..

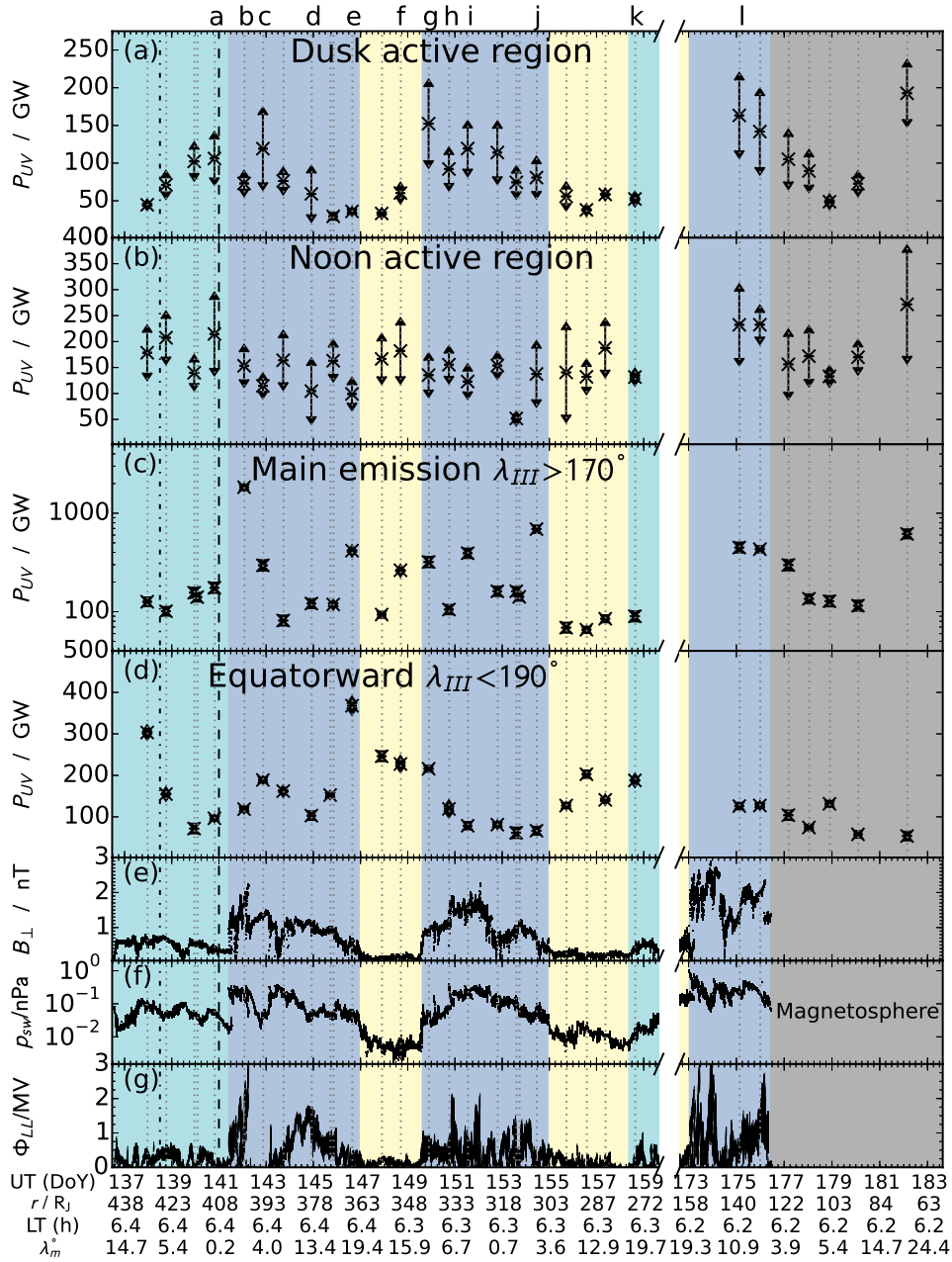


**Figure 3.** Plot showing powers from different auroral regions as labelled, in the same format as Figure 1. Note the log scale in panel (c).

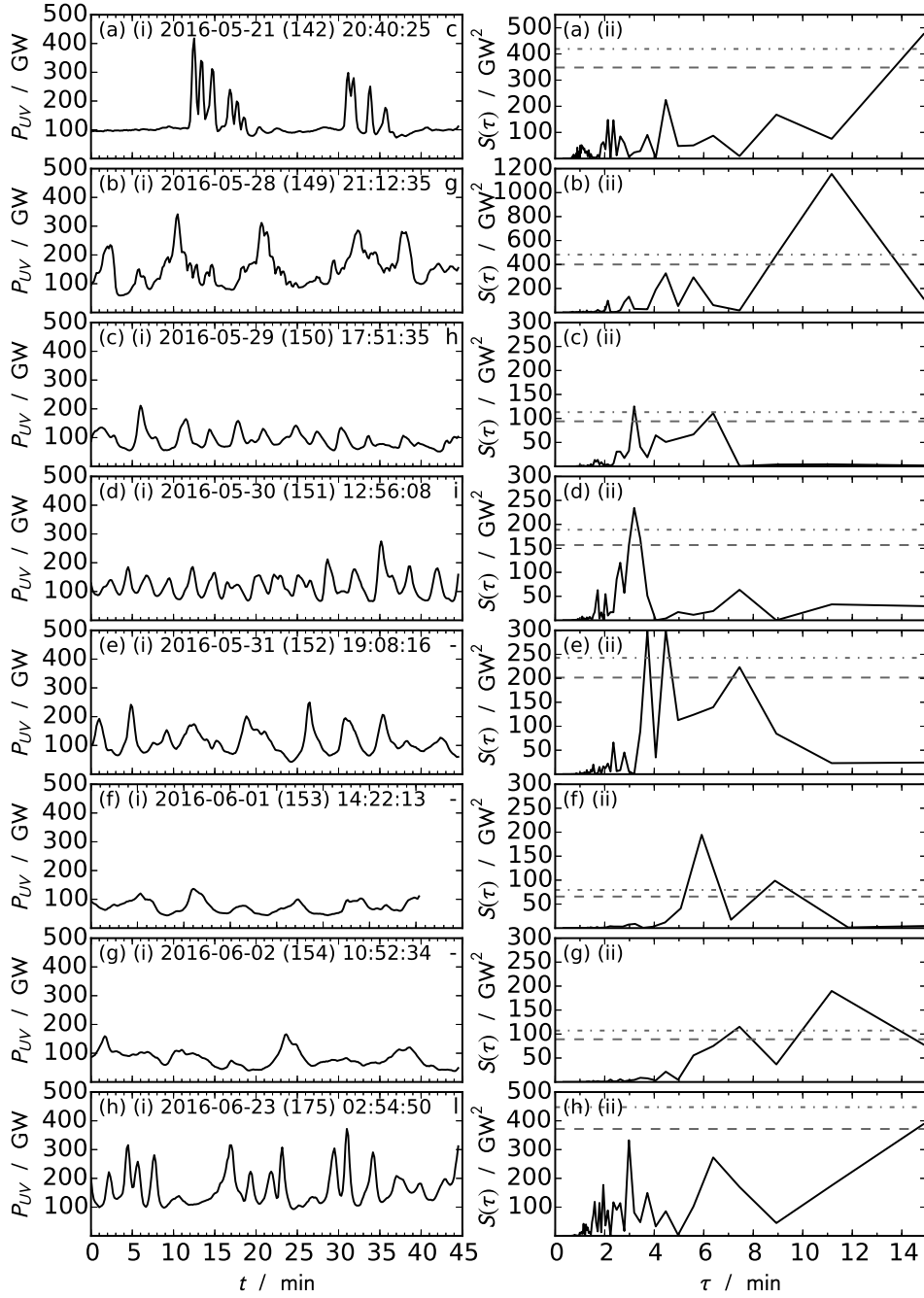


**Figure 4.** Plot showing (left) time series of DAR powers obtained during selected orbits, and (right) power spectra  $S(\tau)$  of the same, computed using fast Fourier transforms. Start times of the observations corrected for one-way light time are given, along with the corresponding image in Figure 2 if applicable. Times  $t$  and periods  $\tau$  are both in units of minutes. Also shown are the 95% and 99% significance levels against the null hypothesis of white noise (gray dashed and dot-dashed lines, respectively).

We now consider the low longitude equatorward (LLEQ) emission, the powers for which are shown in Figure 3d. This region exhibited emission that varied significantly over the program, with values of  $\sim 50$ -350 GW, peaking on DoY 146. The emission was initially principally located in the ‘kink’ region (Figure 2c), then taking the form of a secondary arc (Figure 2d), and the high powers on DoYs 146-149 corresponded to patchy emission of varying intensity, in some cases overlapping and extending down from the main emission, as discussed previously by *Radioti et al.* [2009]; *Nichols et al.* [2009a]; *Dumont et al.* [2015] and *Gray et al.* [2016]. Superficially, the equatorward powers seem to be enhanced in rarefaction regions though, with no significant correlations with any interplanetary parameter, this is not a robust result.

#### 4 Discussion and Summary

We have presented the first set of HST observations made simultaneously with an extended and complete set of near-Jupiter interplanetary data, obtained by the Juno spacecraft. During the HST program Juno observed 3 compression regions in the interplanetary medium, interspersed by rarefaction regions of varying depth. We showed that:

- During the compressions (at least for  $\sim 1$ -3 days after each onset) the well-defined main emission usually observed by HST on the dawn side and a region poleward of the main emission on the dusk side exhibited enhanced powers, with the latter comprising bursty or periodic patches and arcs parallel to the main emission. This poleward dusk emission was also active during the shallow rarefaction at the start of the interval.
- During the second compression, the dusk emission was quasi-periodic, with spectral peaks broadening and moving toward longer periods during the compression.
- The noon active region exhibited transient emission during both rarefactions and compressions, though during compressions the emission was typically a noonward extension of the dusk active region emission, while during the rarefactions (and the later region of the first compression) the emission was either generally unstructured or formed an arc poleward of the main emission.
- The auroras equatorward of the main emission at low longitudes exhibited a broad increase and decrease in power over an interval of  $\sim 10$  days following the sodium nebula enhancement, initially exhibiting enhanced intensity in the dusk sector, then a prominent secondary arc, and finally bright patches of aurora overlapping the main emission.

The brightening of the WDME in response to compression region onset is confirmed, and remains to be fully explained. Theoretical studies have indicated that the main oval should dim in response to compressions, with caveats concerning ionospheric response times [*Southwood and Kivelson, 2001; Cowley et al., 2007*], though recently *Chané et al.* [2017] have shown that at least the nightside main emission could brighten during compressions owing to enhanced magnetospheric asymmetries. Previous observations of small-scale poleward nightside flashing spots have been attributed to nightside reconnection [*Grodent et al., 2004*], and the pulsating DAR emission is possibly a manifestation of larger scale dusk/nightside compression-induced reconnection as part of the Vasylunas or Dungey cycles. Additionally, the active DAR emissions during the initial shallow rarefaction is interesting and is either a response to ongoing activity at Io or the solar wind, noting that the IMF strength during this interval is significantly higher than that observed during the deep rarefaction. The extreme dawn storm/compression event observed on DoY 142 is likely a rarefaction of increased mass loading from Io coupled with a coincident onset of a compression region. Enhanced activity on Io is known to affect Jupiter’s magnetosphere and auroras [*Bonfond et al., 2012; Yoneda et al., 2010*], and the brightening of the low latitude emissions over the  $\sim 10$  days following the sodium nebula enhancement possibly indicates the overall time scale for radial transport in Jupiter’s magnetosphere

[Louarn *et al.*, 2014; Gray *et al.*, 2016], though it is also consistent with the conclusions of Mauk *et al.* [1999] that clustered energetic particle injections are associated with solar wind rarefactions. The lack of a correlation between the NAR powers and any interplanetary parameters (e.g.  $v_{sw}$  or  $B_{\perp}$ ) was surprising, but as noted above the morphology was typically distinct between compressions and rarefactions. It seems that the NAR region is neither driven simply by Kelvin-Helmholtz instability at the magnetopause, nor reconnection according to the coupling function used here. Overall, these results evince a dependance of Jupiter's auroras on the interplanetary medium, which thus acts to trigger magnetospheric activity, but that this more complex than previously thought.

### Acknowledgments

This work is based on observations made with the NASA/ESA Hubble Space Telescope (program GO 14105), obtained at STScI, which is operated by AURA, Inc. for NASA. Work at Leicester was supported by STFC Fellowship (ST/I004084/1) and STFC Grant ST/K001000/1. SVB was supported by STFC Grant ST/M005534/1. JTC was supported by grant HST-GO-14105.002-A from STScI to Boston University. Data are available at the MAST Archive (HST), and Wilson *and al* [2017] and McComas *et al.* [2017] (Juno).

### References

- Badman, S. V., and S. W. H. Cowley (2007), Significance of Dungey-cycle flows in Jupiter's and Saturn's magnetospheres, and their identification on closed equatorial field lines, *Ann. Geophysicae*, 25(4), 941–951.
- Badman, S. V., B. Bonfond, M. Fujimoto, R. L. Gray, Y. Kasaba, S. Kasahara, T. Kimura, H. Melin, J. D. Nichols, A. J. Steffl, C. Tao, F. Tsuchiya, A. Yamazaki, M. Yoneda, I. Yoshioka, and K. Yoshioka (2016), Weakening of Jupiter's main auroral emission during January 2014, *Geophys. Res. Lett.*, 43(3), 988–997, doi:10.1002/2015GL067366.
- Baron, R. L., T. Owen, J. E. P. Connerney, T. Satoh, and J. Harrington (1996), Solar wind control of Jupiter's  $H_3^+$  Auroras, *Icarus*, 120(2), 437–442, doi:10.1006/icar.1996.0063.
- Bonfond, B., D. Grodent, J.-C. Gérard, T. S. Stallard, J. T. Clarke, M. Yoneda, A. Radioti, and J. Gustin (2012), Auroral evidence of Io's control over the magnetosphere of Jupiter, *Geophys. Res. Lett.*, 39(1), L01,105–n/a, doi:10.1029/2011GL050253.
- Bonfond, B., D. Grodent, S. V. Badman, J.-C. Gérard, and A. Radioti (2017), Dynamics of the flares in the active polar region of Jupiter, *Geophys. Res. Lett.*, *in press*.
- Brice, N. M., and G. A. Ioannidis (1970), The magnetospheres of Jupiter and Earth, *Icarus*, 13(2), 173–183, doi:10.1016/0019-1035(70)90048-5.
- Chané, E., J. Saur, R. Keppens, and S. Poedts (2017), How is the Jovian Main Auroral Emission Affected by the Solar Wind?, *J. Geophys. Res.*, *in press*.
- Clarke, J. T., D. Grodent, S. W. H. Cowley, E. J. Bunce, P. M. Zarka, J. E. P. Connerney, and T. Satoh (2004), Jupiter's aurora, in *Jupiter: The Planet, Satellites and Magnetosphere*, edited by F. Bagenal and W. B. McKinnon, pp. 639–670, Cambridge. Univ. Press, Cambridge, UK.
- Clarke, J. T., J. D. Nichols, J.-C. Gérard, D. Grodent, K. C. Hansen, W. S. Kurth, G. R. Gladstone, J. Duval, S. Wannawichian, E. J. Bunce, S. W. H. Cowley, F. J. Crary, M. K. Dougherty, L. Lamy, D. G. Mitchell, W. R. Pryor, K. D. Retherford, T. S. Stallard, B. Zieger, P. M. Zarka, and B. Cecconi (2009), Response of Jupiter's and Saturn's auroral activity to the solar wind, *J. Geophys. Res.*, 114(A), A05,210, doi:10.1029/2008JA013694.
- Connerney, J. E. P., J. B. Bjarno, T. Denver, M. Benn, J. Espley, J. L. Jorgensen, P. S. Jorgensen, P. Lawton, A. Malinnikova, J. M. Merayo, S. Murphy, J. Odom, R. Oliverson, R. Schurr, D. Sheppard, and E. J. Smith (), The Juno Magnetic Field Investigation, *Space Sci. Rev.*, doi:10.1007/s11214-017-0334-z.
- Connerney, J. E. P., M. H. Acuña, and N. F. Ness (1981), Modeling the Jovian current sheet and inner magnetosphere, *J. Geophys. Res.*, 86, 8370–8384.

- Connerney, J. E. P., M. H. Acuña, N. F. Ness, and T. Satoh (1998), New models of Jupiter's magnetic field constrained by the Io flux tube footprint, *J. Geophys. Res.*, *103*(A6), 11,929–11,940, doi:10.1029/97JA03726.
- Cowley, S. W. H., J. D. Nichols, and D. J. Andrews (2007), Modulation of Jupiter's plasma flow, polar currents, and auroral precipitation by solar wind-induced compressions and expansions of the magnetosphere: a simple theoretical model, *Ann. Geophysicae*, *25*, 1433–1463.
- Cowley, S. W. H., S. V. Badman, S. M. Imber, and S. E. Milan (2008), Comment on “Jupiter: A fundamentally different magnetospheric interaction with the solar wind” by D. J. McComas and F. Bagenal, *Geophys. Res. Lett.*, *35*(10), L10,101, doi:10.1029/2007GL032645.
- Delamere, P. A., and F. Bagenal (2010), Solar wind interaction with Jupiter's magnetosphere, *J. Geophys. Res.*, *115*(A), A10,201, doi:10.1029/2010JA015347.
- Dumont, M., D. Grodent, A. Radioti, B. Bonfond, and J.-C. Gérard (2015), Jupiter's equatorward auroral features: Possible signatures of magnetospheric injections, pp. 1–10, doi:10.1002/(ISSN)2169-9402.
- Dunn, W. R., G. Branduardi-Raymont, R. F. Elsner, M. F. Vogt, L. Lamy, P. G. Ford, A. J. Coates, G. R. Gladstone, C. M. Jackman, J. D. Nichols, I. J. Rae, A. Varsani, T. Kimura, K. C. Hansen, and J. M. Jasinski (2016), The impact of an ICME on the Jovian X-ray aurora, *Journal of Geophysical Research: Space Physics*, *121*(3), 2274–2307, doi:10.1002/2015JA021888.
- Gray, R. L., S. V. Badman, and B. Bonfond (2016), Auroral evidence of radial transport at Jupiter during January 2014, *J. Geophys. Res.*, *121*, doi:10.1002/(ISSN)2169-9402.
- Grodent, D., J. T. Clarke, J. H. Waite Jr, S. W. H. Cowley, J.-C. Gérard, and J. Kim (2003), Jupiter's polar auroral emissions, *J. Geophys. Res.*, *108*(A10), 1366, doi:10.1029/2003JA010017.
- Grodent, D., J.-C. Gérard, J. T. Clarke, G. R. Gladstone, and J. H. Waite Jr (2004), A possible auroral signature of a magnetotail reconnection process on Jupiter, *J. Geophys. Res.*, *109*(A18), 5201, doi:10.1029/2003JA010341.
- Gustin, J., B. Bonfond, D. Grodent, and J.-C. Gérard (2012), Conversion from HST ACS and STIS auroral counts into brightness, precipitated power, and radiated power for H<sub>2</sub> giant planets, *J. Geophys. Res.*, *117*(A7), A07,316, doi:10.1029/2012JA017607.
- Joy, S. P., M. G. Kivelson, R. J. Walker, K. K. Khurana, C. T. Russell, and T. Ogino (2002), Probabilistic models of the Jovian magnetopause and bow shock locations, *J. Geophys. Res.*, *107*(A10), SMP 17–1–SMP 17–17, doi:10.1029/2001JA009146.
- Khurana, K. K., M. G. Kivelson, V. M. Vasyliūnas, N. Krupp, J. Woch, A. Lagg, B. H. Mauk, and W. S. Kurth (2004), The configuration of Jupiter's magnetosphere, in *Jupiter: The Planet, Satellites and Magnetosphere*, edited by F. Bagenal, T. E. Dowling, and W. B. McKinnon, pp. 593–616, Cambridge Univ. Press.
- Kimura, T., and et al. (2017), Auroral explosion at Jupiter observed by the Hisaki satellite and Hubble Space Telescope, *Geophys. Res. Lett.*, *submitted*.
- Kimura, T., R. P. Kraft, R. F. Elsner, G. Branduardi-Raymont, G. R. Gladstone, C. Tao, K. Yoshioka, G. Murakami, A. Yamazaki, F. Tsuchiya, M. F. Vogt, A. Masters, H. Hasegawa, S. V. Badman, E. Roediger, Y. Ezoe, W. R. Dunn, I. Yoshikawa, M. Fujimoto, and S. S. Murray (2016), Jupiter's X-ray and EUV auroras monitored by Chandra, XMM-Newton, and Hisaki satellite, *Journal of Geophysical Research: Space Physics*, *121*(3), 2308–2320, doi:10.1002/2015JA021893.
- Kita, H., T. Kimura, C. Tao, F. Tsuchiya, H. Misawa, T. Sakanoi, Y. Kasaba, G. Murakami, K. Yoshioka, A. Yamazaki, I. Yoshikawa, and M. Fujimoto (2016), Characteristics of solar wind control on Jovian UV auroral activity deciphered by long-term Hisaki EXCEED observations: Evidence of preconditioning of the magnetosphere?, *Geophys. Res. Lett.*, *43*(1), 6790–6798, doi:10.1002/2016GL069481.
- Louarn, P., C. P. Paranicas, and W. S. Kurth (2014), Global magnetodisk disturbances and energetic particle injections at Jupiter, *Journal of Geophysical Research: Space Physics*,

- 119(6), 4495–4511, doi:10.1002/2014JA019846.
- Mauk, B. H., D. J. Williams, R. W. McEntire, K. K. Khurana, and J. G. Roederer (1999), Storm-like dynamics of Jupiter’s inner and middle magnetosphere, *J. Geophys. Res.*, *104*(A10), 22,759–22,778, doi:10.1029/1999JA900097.
- McComas, D. J., and F. Bagenal (2007), Jupiter: A fundamentally different magnetospheric interaction with the solar wind, *Geophys. Res. Lett.*, *34*(20), L20,106, doi:10.1029/2007GL031078.
- McComas, D. J., N. Alexander, F. Allegrini, F. Bagenal, C. Beebe, G. Clark, F. J. Crary, M. I. Desai, A. De Los Santos, D. Demkee, J. Dickinson, D. Everett, T. Finley, A. Gribanova, R. Hill, J. Johnson, C. Kofoed, C. Loeffler, P. Louarn, M. Maple, W. Mills, C. Pollock, M. Reno, B. Rodriguez, J. Rouzaud, D. Santos-Costa, P. Valek, S. Weidner, P. Wilson, R. J. Wilson, and D. White (2013), The Jovian Auroral Distributions Experiment (JADE) on the Juno Mission to Jupiter, *Space Sci. Rev.*, doi:10.1007/s11214-013-9990-9.
- McComas, D. J., J. R. Szalay, F. Allegrini, F. Bagenal, S. J. Bolton, J. E. P. Connerney, R. W. Ebert, G. R. Gladstone, W. S. Kurth, S. M. Levin, P. Louarn, B. H. Mauk, C. Pollock, M. Reno, M. F. Thomsen, P. Valek, S. Weidner, and R. J. Wilson (2017), Plasma environment at the dawn flank of Jupiter’s magnetosphere: Juno arrives at Jupiter, *Geophys. Res. Lett.*, *submitted*.
- Nichols, J. D., S. W. H. Cowley, and D. J. McComas (2006), Magnetopause reconnection rate estimates for Jupiter’s magnetosphere based on interplanetary measurements at ~5AU, *Ann. Geophysicae*, *24*, 393–406.
- Nichols, J. D., E. J. Bunce, J. T. Clarke, S. W. H. Cowley, J.-C. Gérard, D. Grodent, and W. R. Pryor (2007), Response of Jupiter’s UV auroras to interplanetary conditions as observed by the Hubble Space Telescope during the Cassini flyby campaign, *J. Geophys. Res.*, *112*(A11), A02,203, doi:10.1029/2006JA012005.
- Nichols, J. D., J. T. Clarke, J.-C. Gérard, D. Grodent, and K. C. Hansen (2009a), Variation of different components of Jupiter’s auroral emission, *J. Geophys. Res.*, *114*(A6), A06,210, doi:10.1029/2009JA014051.
- Nichols, J. D., J. T. Clarke, J.-C. Gérard, and D. Grodent (2009b), Observations of Jovian polar auroral filaments, *Geophys. Res. Lett.*, *36*(8), L08,101, doi:10.1029/2009GL037578.
- Pallier, L., and R. Prangé (2001), More about the structure of the high latitude Jovian aurorae, *Planet. Space Sci.*, *49*(10-11), 1159–1173, doi:10.1016/s0032-0633(01)00023-x.
- Pryor, W. R., A. I. F. Stewart, L. W. Esposito, W. E. McClintock, J. E. Colwell, A. J. Jouchoux, A. J. Steffl, D. E. Shemansky, J. M. Ajello, R. A. West, C. J. Hansen, B. T. Tsurutani, W. S. Kurth, G. B. Hospodarsky, D. A. Gurnett, K. C. Hansen, J. H. Waite Jr, F. J. Crary, D. T. Young, N. Krupp, J. T. Clarke, D. Grodent, and M. K. Dougherty (2005), Cassini UVIS observations of Jupiter’s auroral variability, *Icarus*, *178*(2), 312–326, doi:10.1016/j.icarus.2005.05.021.
- Radioti, A., A. T. Tomas, D. Grodent, J.-C. Gérard, J. Gustin, B. Bonfond, N. Krupp, J. Woch, and J. D. Menietti (2009), Equatorward diffuse auroral emissions at Jupiter: Simultaneous HST and Galileo observations, *Geophys. Res. Lett.*, *36*(7), n/a–n/a, doi:10.1029/2009GL037857.
- Southwood, D. J., and M. G. Kivelson (2001), A new perspective concerning the influence of the solar wind on the Jovian magnetosphere, *J. Geophys. Res.*, *106*(A4), 6123–6130, doi:10.1029/2000JA000236.
- Stallard, T. S., J. T. Clarke, H. Melin, S. Miller, J. D. Nichols, J. O’Donoghue, R. E. Johnson, J. E. P. Connerney, T. Satoh, and M. Perry (2016), Stability within Jupiter’s polar auroral ‘Swirl region’ over moderate timescales, *Icarus*, *268*, 145–155, doi:10.1016/j.icarus.2015.12.044.
- Tao, C., T. Kimura, S. V. Badman, N. Andre, F. Tsuchiya, G. Murakami, K. Yoshioka, I. Yoshikawa, A. Yamazaki, and M. Fujimoto (2016), Variation of Jupiter’s aurora observed by Hisaki/EXCEED: 2. Estimations of auroral parameters and magnetospheric

dynamics, *Journal of Geophysical Research: Space Physics*, 121(5), 4055–4071, doi: 10.1002/2015JA021272.

Wilson, R. J., and al (2017), Solar Wind Properties During Juno's approach to Jupiter: 1. Data Analysis and Resulting Plasma Properties Utilizing a 1D Forward model, *Geophys. Res. Lett.*, *submitted*.

Yoneda, M., H. Nozawa, H. Misawa, M. Kagitani, and S. Okano (2010), Jupiter's magnetospheric change by Io's volcanoes, *Geophys. Res. Lett.*, 37(11), n/a–n/a, doi: 10.1029/2010GL043656.